Imputation techniques for the detection of microstructural changes in schizophrenia, with an application to magnetization transfer imaging.

Silke Bachmann[a], Sebastian Haffer[b], Petra Beschoner[c], Roberto Viviani[b]

[a] Dept. of Psychiatry, Psychotherapy, and Psychosomatics, University of Halle (Saale), Germany
[b] Dept. of Psychiatry and Psychotherapy III, University of Ulm, Germany
[c] Dept. of Psychosomatic Medicine and Psychotherapy, University of Ulm, Germany

Corresponding author
Roberto Viviani, PhD
Department of Psychiatry and Psychotherapy III
University of Ulm,
Leimgrubenweg 12
89075 Ulm
Germany

email: roberto.viviani@uni-ulm.de

NOTICE: this is the author's version of a work that was accepted for publication in Schizophrenia Research. Changes resulting from the publishing process, such as peer review, editing, corrections, structural formatting, and other quality control mechanisms may not be reflected in this document. Changes may have been made to this work since it was submitted for publication. A definitive version was subsequently published in Schizophrenia Research, [132:91-96, 2011 Oct] DOI: doi:10.1016/j.schres.2011.07.023.

Abstract

Neuroimaging techniques such as magnetization transfer imaging allow the detection of microstructural alterations of tissue, and for this reason have been applied to the study of disorders such as schizophrenia. However, they are also sensitive to partial volume effects arising from mixed compartments, such as those comprising cerebral spinal fluid, which makes separate evaluation of volumetric and structural alterations difficult. Ensuing regional differences in the distribution of data and signal-to-noise ratio add further potential bias to their assessment. In the present study we simultaneously applied tissue segmentation, statistical imputation, and nonparametric inference to address these issues and improve the validity of statistical inference. In a case study of *N*=32 schizophrenic patients matched to the same number of controls, we compared a standard voxel-based analysis with one supplemented by the imputation technique. We were able to replicate significant results in the imputed analysis and even extend them in the areas not excluded by excessive partial volume effects. Application of segmentation algorithms in this dataset also suggested that partial volume effects from spinal fluid potentially affect inference in most cortical gray matter, unless remedial steps are undertaken. Refined imputation methods may be particularly attractive in future research settings characterized by large samples and the availability of adequate computational resources.

KEYWORDS: imputation, voxel-based analysis, magnetization transfer imaging, partial volume effect, schizophrenia

1. Introduction

Structural brain changes associated with schizophrenia have been detected both with techniques explicitly assessing volumetric abnormalities (Bachmann et al., 2003, 2004, 2007; Shenton et al. 2001; Wright et al. 2000) and with approaches that combined statistical parametric mapping (SPM) and voxelwise structural indices, such as voxel-based morphometry (VBM) (Ashburner and Friston, 2000; Honea et al., 2008; Nagai et al., 2007; Pomarol-Clotet et al., 2010). Reviews and meta-analyses (Shenton et al. 2001; Wright et al., 2000) reliably report increases in ventricular size, especially in the third and lateral ventricles, as well as reduced brain tissue - mostly white matter - in the temporal lobes including the amygdala, hippocampus, parahippocampal gyrus, superior temporal gyrus, and frontal lobes and substructures of patients. Claims regarding other structures such as parietal lobe, cerebellum, and the corpus callosum remain more disputed (Bachmann et al., 2003; Bottmer et al., 2005; Shenton et al., 2001; Wright et al., 2000).

More recent approaches involve specialized neuroimaging techniques such as diffusion-weighted imaging and magnetization transfer imaging (MTI). With respect to morphometric studies, they raise the question of whether they confirm established findings, or may add any novel insight on tissue changes accompanying pathology. Because their signal is sensitive to microstructural changes and tissue integrity, these techniques may detect alterations even in the absence of manifest volumetric abnormalities, thus complementing morphometric studies. However, their sensitiveness to microstructural abnormalities also makes it possible to investigate a different dimension of structural change, which ideally would be assessed independently of volumetric changes. In this case, the influence of signal from cerebrospinal fluid (CSF) on these images, which may conceivably reflect larger

extraparenchymal volume even when the brain tissue is qualitatively unaltered, becomes a confounder.

The purpose of this study is to report on the combined application within the voxel-based framework of the techniques of probabilistic tissue segmentation (Ashburner and Friston, 1997) and imputation (Little and Rubin, 2002) to contain partial volume effects (PVEs) due to CSF. Such PVEs may lead to signal changes unrelated to microstructural abnormalities. The problem is especially acute at the borders of CSF and parenchyma, where some voxels cannot be assigned to one category unequivocally. In the presence of larger CSF volumes in schizophrenic patients, expanded contact areas may increase the likelihood for PVEs to occur (Wright et al., 2000).

Imputation is a statistical technique to rebuild an unbiased full dataset in the presence of missing data (Little and Rubin, 2002). In the present application, the data are not missing or lost but discarded after being declared invalid due to the contribution of partial volume effects, as detected in an independent segmentation. The advantages to analysis are manifold: capacity to discriminate between different sources of signal changes, such as those arising from enlarged CSF and those attributable to microstructural changes; improved distributional properties of the data, which no longer arise from a mixture of compartments; reduced signal variance and as a consequence improved detection power.

In the case study, we applied imputation to compare schizophrenic patients and healthy controls scanned with magnetization transfer imaging (MTI, Henkelman et al., 2001). First described by Wolff and Balaban (1989), this specialized imaging technique has also been applied to the study of structural changes in schizophrenia, resulting in the detection of signal decreases (Konrad and Winterer, 2008). Like diffusion-weighted imaging (Kubicki et al., 2005), MTI is more sensitive to early and

subtle microstructural changes than conventional MRI. For this reason, typical applications of MTI involve assessment of white matter lesions as in multiple sclerosis (Filippi and Agosta, 2009). Whereas diffusion-weighted imaging techniques only assess white matter integrity, MTI detects abnormalities in both white and gray matter. MTI is sensitive to the interaction of protons bound to macromolecular structures with tissue water. Brain macromolecules, i.e. glial membrane proteins and phospholipids in gray matter as well as myelin or axons in white matter, can be saturated using an off-resonance radiofrequency pulse. The following desaturation – either directly or via chemical exchange – can be measured in percentage units as magnetization transfer ratio (MTR) (Henkelman et al., 2001). Hence, MTR is a quantitative measure of macromolecular structural integrity, in which high signal levels correspond to a larger fraction of macromolecules in tissue (Konrad and Winterer, 2008).

After describing – in the Material and Methods section – the details of the imputation approach to contain PVEs in the voxel-based framework, we will report on two analyses of the same data. The first analysis, conducted on the *original dataset,* limited PVEs by using a mask based on *a priori* estimates of the probability of CSF occurrences in each voxel. Data were not submitted to imputation, and the analysis followed a conventional approach. The second analysis on an *imputed dataset* implemented PVE control by exploiting segmentation information tailored on the distribution of the CSF compartment in each participant. Furthermore, to counter possible problems due to the non-normal distribution of data (Viviani et al., 2007), significance levels were estimated non-parametrically using a permutation technique (Holmes et al., 1996). Two issues were of interest. The first was assessing the extension of the volume potentially affected by PVEs, and the amount of this volume that could be rescued from PVEs by imputation. The second was whether any

differences detected in the patient group in the traditional analysis were still present after imputation and the use of nonparametric tests, which make inference robust to distributional misspecification.

2. Materials and Methods

2.1 Patients and controls subjects

Thirty-two patients (21 male, 12 female; 33.1 years ±8.6) in treatment at the Department of Psychiatry III, University of Ulm, and 32 age- and sex-matched healthy control subjects (21 male, 12 female; 33.5 years ±10.1 years) were included into the study after they gave written informed consent (logistic regression: age, $z = -0.21$, $p=0.83$; sex, $z = -0.10$, $p=0.92$). Patients were hospitalized for an episode of schizophrenia or schizoaffective disorder according to DSM-IV (American Psychiatric Association, 1994). Two psychiatrists independently confirmed the diagnoses. The mean number of illness episodes amounted to 3 (SD 2.3, range 1-11). All patients were in partial remission and psychopathologically stable. Treatment consisted of atypical antipsychotics. Automated methods (Rosenbaum, 2009) were used to select matched controls from a larger database of 106 individuals from which MTI images were concurrently obtained (mean age 26.0 years ±8.0, 40 males). The study was conducted in accordance with the Declaration of Helsinki and formally approved by the Ethical Review Board of the University of Ulm. Inclusion criteria for both groups were Caucasian ethnicity, age between 18 and 55 years, right-handedness (Oldfield et al. 1971). Besides applying the general exclusion criteria for MRI, subjects with MR abnormalities, a past history of or a concomitant psychiatric, neurological or severe medical disorder, and substance abuse were excluded following a thorough interview.

2.2 Image acquisition

Neuroimaging data were acquired with a 3T Allegra scanner (Siemens AG, Erlangen) equipped with a standard head coil. T2-weighted images (TE/TR/voxel size = 12ms/1000ms/0.43×0.43×6mm^3) were obtained to exclude gross structural abnormalities. For magnetization transfer imaging, two datasets were acquired (TE/TR/voxel size = 12ms/700m/0.86×0.86×5.5mm^3) with (M_s) and without (M_0) saturation pulse. Resolution of the image matrix was 256x256 voxels with a bandwidth of 110 Hz/voxel. Altogether, 24 transversal slices with 0.5 mm interslice space were acquired. The final data set consisting of the magnetization transfer ratio (MTR) as an index of macromolecule loss was calculated voxel by voxel using the formula: MTR=([$M_0 – M_s$]/M_0)x100 percent units (Henkelman et al., 2001).

2.3 Preprocessing

Affine realignment between M_0 and M_s images was performed in each subject with SPM5 software (Wellcome Department of Cognitive Neurology, London, UK) using the average image as target. An integrated normalization-segmentation procedure (Ashburner and Friston, 1997) was conducted on the M_0 image without saturation pulse (which is a T1-weighted image without magnetization transfer effects) on the T1-weighted ICBM-MNI template (Montreal Neurological Institute), and the resulting normalization parameters applied to the MTR image. Normalization-segmentation outputted voxelwise maps of estimated probabilities to belong to the gray matter (GM), white matter (WM), or the cerebrospinal fluid (CSF) compartment to be used in the imputation procedure. Data were smoothed with a Gaussian kernel (full width at half-maximum, FWHM, 3x3x5 mm).

2.4 Data analysis and description of the imputation procedure

To assess the impact of imputation, two parallel analyses were conducted on the same dataset and volume of interest. The first was a standard SPM analysis on the original dataset. This approach is based on Gaussian random field theory (Worsley et al., 1992; Friston 1996), which was used to test the null hypothesis of no reduction in MTR values in the patient group voxelwise, with age and gender serving as covariates. Prior to testing, data were masked by excluding voxels that, according to the *a priori* segmentation maps delivered with the SPM software, had a probability of 0.15 or larger to belong to the CSF compartment. The cerebellum was excluded from all analyses because affected by loss of coverage in some scans.

In the second, imputed analysis an individually tailored mask was computed by excluding voxels that could be assigned to CSF with a probability of 0.15 or more, according to the normalization-segmentation step. Due to the variable configuration and course of most sulci at a given voxel location (Van Essen and Dierker, 2007; Zilles et al., 1997) the data may be assigned to CSF in some individuals but not in others (*CSF datapoints*). After being discarded, such CSF datapoints were considered as 'missing data' and handled by 'simple imputation' (Little and Rubin, 2002) to reconstitute a full dataset as required by the voxel-based approach. In each voxel where they occurred, discarded CSF datapoints were replaced by values generated at random according to a normal distribution with mean and variance estimated from the datapoints in the same voxel that had not been assigned to CSF (*non-CSF datapoints*). Because classification of tissue was obtained from the M_0 volumes where the MTR information was absent, it contained volumetric information as would be acquired in by voxel-based morphometry. Because means and variances of the imputed values' distribution must be estimated from non-CSF datapoints, voxels with less than 24 non-CSF datapoints in each group were

excluded from analysis to ensure reasonably large samples for these estimates. This threshold was chosen pragmatically as a compromise between good volume coverage and number of available non-CSF datapoints (75% of the sample). After imputation, data were smoothed. A supplementary analysis, to which we refer briefly in the Results, was conducted with the more stringent CSF threshold of 0.05 and correspondingly smaller volume coverage.

Note that two properties of the imputation procedure are essential to avoid bias in model estimates (Little and Rubin, 2002). The first is the generation of data at random according to a model that preserves the variance of the data. Here, this model was given by the group-level mean and variance estimated from the non-CSF datapoints. In contrast, a naïve approach that does not make use of random data, for example replacing missing data with the means of available data, artifactually reduces residual variance, inflating the test statistic. The second property is the separate imputation in the two groups, which preserves expected differences between group means (for detailed discussion, see Little and Rubin, 2002).

To address the possible influence of non-normality of MTR values on statistical inference, datapoints in this second analysis were ranked in each voxel separately and tested with a permutation technique (Holmes et al., 1996, Nichols and Holmes, 2002) to obtain voxel-level (strong) correction of significance values. Ranking and imputation complement each other to obtain a more homogeneous data distribution across the volume under the null. Computational feasibility prevented us from repeating the imputation at each permutation step, which would have fully accounted for the mild overdispersion induced by finite-sample estimates of distributional parameters used in imputation. Ranking may also alleviate this concern.

3. Results

3.1 Volume coverage in the original and imputed datasets

Figure 1, left, shows the mask applied to the original dataset, which was the same in all participants and consisted of the *a priori* map of CSF probabilities thresholded at 0.15. The center of the same Figure shows the volume coverage in the imputed dataset, in which the threshold of 0.15 was applied individually before imputing CSF datapoints (yellow). The volume coverage would have been much smaller if no imputation had been used and the analysis had included only voxels below the 0.15 threshold in all individuals (light blue). One can see that most gray matter may have been affected by CSF signals at the 0.15 threshold, and that imputation extended volume coverage to this compartment. The right part of Figure 1 illustrates the further reduction of volume coverage in an imputed dataset at the more stringent CSF threshold of 0.05; at this threshold, only part of the gray matter is available for analysis.

FIGURE 1

The imputation procedure at the 0.15 threshold replaced 7213 CSF datapoints per volume on average (in the control group, 7263±2026; in the patient group, 7171±2774; Wilcoxon rank sum test for independent samples: z=0.32, p=0.74). Figure 2 (left) illustrates the regional occurrence of imputed datapoints in the control and patient groups. The distribution of the data in the imputed regions became less spread-out, as one may expect from discarding highly variable CSF signal (Figure 2 right).

FIGURE 2

3.2 Original dataset, SPM analysis

Comparison of voxel-based MTR signals yielded reductions in the patient group in several areas, but were more prominent in the right hemisphere (Figure 3, top row). All significance values reported here were corrected for the whole volume coverage at voxel level (strong correction for multiple testing). The most extensive reductions affected the right temporal lobe, involving the white matter posterior to the internal capsule (Mori et al., 2005) and the adjacent calcarine and fusiform cortex (see Table 1 for details). Some of these areas were affected on the left as well. Reductions also affected circumscribed areas at the border with the adjacent white matter in the hippocampus, the lingula, the anterior cingulate gyrus, at the border. Isolated changes were detected in the insula and pallidum.

FIGURE 3

TABLE 1

3.3 Imputed dataset, permutation test after ranking

The analysis of the imputed dataset confirmed the changes in the temporal lobe (see Figure 3, bottom row, and Table 2). In contrast, in the anterior cingulate region the effect in the imputed analysis was shifted away from the midline, because some of the voxels in this position were too affected by PVEs to be included in the imputed dataset. In the posterior insular region, the imputed dataset was better than the original dataset at detecting signal decreases, resulting in newly detected clusters, such as those in BA20-21 and in the right Rolandic operculum, BA48. Additional effects were detected in parts of the middle frontal gyrus (BA46). In contrast, the isolated effects in the insula and putamen were not confirmed in the imputed dataset, due to the high CSF probability assigned to these voxels.

TABLE 2

A supplementary analysis with imputed data after strict CSF control at the threshold 0.05 gave very similar results (see Table S1 in the supplementary material available online). However, the much reduced coverage of this supplementary analysis, as shown in Figure 1, right, resulted in detecting less foci in gray matter compared to the analysis at the more lenient PVE threshold.

4. Discussion

4.1 Substantive findings

While the main focus of the present work was methodological, we consider it appropriate to comment briefly on our findings with respect to the existing literature. Our data confirm findings in the literature of possible changes in the temporal lobe and parts of the prefrontal cortex, but we failed to replicate the finding of changes in the corpus callosum. The insular regions were shown to be too prone to possible PVE to be amenable to analysis.

Overall, results of MTI studies exhibit a broad variability, likely as a consequence of widespread use of uncorrected significance thresholds (Beschoner et al., 2005). The most consistent findings affect the insular cortex, the temporal, and the parietal cortex as well as the connecting WM fibers (Antosik-Biernacka et al., 2006; Foong et al., 2001; Kubicki et al., 2005, 2007). Further studies found additional MTR-signal reductions in the right medial prefrontal cortex and the WM extending from the insular cortex to the uncinate fasciculus (Bagary et al., 2003; Mandl et al., 2010; Price et al. 2010), the right occipital region, the left periventricular WM (Antosik-Biernacka et al., 2006) and the corpus callosum (Douaud et al., 2007). Reviews and meta-analyses were undertaken on studies applying VBM to compare schizophrenia patients and healthy controls (Di et al., 2009; Honea et al., 2005; Nagai et al., 2007; Williams, 2008). These studies confirm the existence of WM or WM/GM deficits in patients

relative to controls, among others with respect to frontal and temporal regions (superior temporal gyrus and medial temporal lobe), and the internal capsule. When MTI and VBM are applied together, however, differences between patients and control appear to affect disjoint areas (Price et al. 2010).

In contrast to WM, less attention has been given to correlates of GM abnormalities. Price et al. (2010) reported changes in the superior right prefrontal cortex. Studies that deal with disease exacerbations and medication effects suggest that the GM/WM borders may be affected in schizophrenia patients. Authors reported GM volume decrease in patients who were treated with atypical antipsychotics (Bartzokis et al., 2007; Cahn et al., 2002; Lieberman et al., 2005; Scherk and Falkai, 2006). This effect may explain the localizations straddling WM and GM in our study, but remains to be confirmed.

4.2 Validity of the imputation procedure

Several issues on the validity of the proposed imputation procedure should be mentioned. Firstly, the quality of PVE control depends on the underlying segmentation algorithm. A comparative validation of segmentation algorithms is outside the scope of the present work. The second issue concerns the choice of the threshold at which datapoints are discarded. Higher thresholds offer more protection against contamination from other tissue compartments but reduce volume coverage. While not immediately apparent, this issue is essentially one of data resolution: with larger datasets, compartments may be separated more precisely at the same levels of volume coverage. Stricter thresholds, like higher resolution, can only be good, but come at a cost. Our data suggest that the insular region in particular may require samples larger than ours to be adequately assessed. Finally, with more computational resources available, the imputation procedure adopted here could be

improved by extending it to multiple imputation schemes, and by repeating the imputation at every permutation step. Yet, even the simplified scheme proposed here, with all its imperfections, seems preferable to parametric testing when considering the extremely long tails of the original data distribution visible in Figure 2.

Application of the imputation approach revealed that the findings of the original dataset were confirmed in the regions where there was enough support to reconstruct the dataset with CSF control. The main affected areas were gray and white matter in the temporal and occipital lobes, especially on the right, the parietal operculum, as well as the left middle frontal gyrus in the imputed dataset. This suggests that these reductions were not due to PVEs arising from CSF contamination. In some cases differences appeared larger in the imputed dataset. As the MTR signal in CSF is much lower than in parenchyma, the exclusion of CSF voxels may eliminate a source of heterogeneous variance from the data, thus improving the signal to noise ratio whenever true differences in MTR are present.

4.3 Conclusion

Combined with segmentation, imputation techniques may increase the specificity and power of statistical analysis in data aiming at uncovering microstructural changes using voxel-based models. The periinsular areas are strongly affected by PVEs and may require large samples to investigate microstructural changes.

Figure legends

Figure 1. Masks used in the analysis. Left: mask used in the analysis of the original data with the SPM software, obtained by thersholding an *a priori* map of CSF probabilities of less than 0.15, overlaid on a template brain at z=0. Center: the mask used in the main analysis in the imputed dataset (yellow), with the smaller support of the data that were assigned to CSF with probability less than 0.15 in all subjects (blue), and therefore was not subject to imputation. Right: the analogous mask in the supplementary analysis, with a stricter CSF probability threshold of less than 0.05.

Figure 2. Imputation. Left: Maps of the count of imputed datapoints for the main analysis (CSF threshold 0.15) in the control (left) and patient group (right), overlaid on a template brain at z=0. Right: comparative histograms of MTR values in the region defined by 5 or more CSF datapoints (about 43800 voxels), obtained before (top) and after (bottom) imputation. The long tails are visible as a thin dark line along the x axis. Note also that the x axis is differently scaled in the two histograms.

Figure 3. Statistical parametric maps of reduction of MTR in the patient group, thresholded at $p < 0.05$, corrected at voxel level (strong correction) for the whole volume, overlaid on a chimeric template. The right half of the template is a prototypical T1-weighted structural image of the same single individual of previous figures, meant to provide familiar landmarks to the reader for the identification of the locus of effects. The left half of the template is an average MTR image, obtained as the mean of the control sample of N=106, meant to convey the quality of the MTR signal. Brighter values refer to a higher concentration of macromolecules, evident as higher MTR values in white matter. The results of testing differences between patients and controls are shown as an overlay in blue. The top row shows statistically significant MTR reductions in the original dataset, as detected with the SPM software. The bottom row shows statistically significant MTR reductions in the imputed dataset.

Tables

Table 1 Original dataset

Cortical area / white matter structure	Coord. (mm.)	*t*	*p* (corr)
<no cortical voxel>/ sagittal stratum R	30 -58 -12	7.57	<0.001
Calcarine R (BA19) / cingulum R	22 -50 6	7.75	<0.001
Calcarine R (BA17) / cingulum R	18 -58 16	5.97	0.012
Calcarine L (BA17) / cingulum L	-18 -58 18	6.64	0.001
Lingual R (BA27) / cingulum R	12 -48 2	6.95	<0.001
Lingual L (BA27) / cingulum R	-12 -46 2	7.65	<0.001
Precuneus R (BA23)	16 -66 28	6.29	0.003
Precuneus L (BA29)	-6 -46 10	5.83	0.020
Fusiform R (BA20) / sagittal stratum R	48 -38 -26	6.06	0.008
Fusiform R (BA37) / sagittal stratum R	38 -48 -14	5.60	0.047
Fusiform L (BA30) / sagittal stratum L	-16 -42 -10	7.13	<0.001
Fusiform L (BA19) / sagittal stratum L	-28 -72 -16	6.13	0.006
Temporal Inf R (BA37)	46 -58 -22	7.82	<0.001
Rolandic Operc L (BA48)	-38 -28 20	6.44	0.002
Insula R (BA48) / internal capsule	42 -2 -12	6.65	0.001
Hippocampus R (BA20)	28 -22 -12	6.88	<0.001
Hippocampus R (BA35) / cingulum R	14 -10 -14	6.55	0.001
Hippocampus R (BA37)	32 -32 -2	5.81	0.022
Cingular cortex ant L (BA24)	-2 24 22	7.80	<0.001
Pallidum L	-6 4 -2	5.75	0.027

Detected changes in gray and white matter are reported on the left and right of the forward slash sign '/', respectively; some areas consist of gray or white matter only. Gray matter loci are identified by Brodmann area numbers (BA); white matter structures are named after the atlas by Mori et al. (Mori et al., 2005). White matter nomenclature always follows the slash; these names should not be confused with quasi-homonymous gray matter structures. Explanation of symbols: Coord.: coordinates, in millimetres, according to the Montreal Neurological Institute (MNI) standard reference space; *t*: Student's *t*; *p* (corr): significance value, voxel-level (peak-level) corrected for the whole volume; ant, inf: anterior, inferior; L, R: left, right.

Table 2. Imputed dataset

Cortical area / white matter structure	Coord. (mm.)	*t*	*p* (corr.)
<no cortical voxel>/ sagittal stratum R	24 -76 -12	8.152	<0.001
Calcarine R (BA19) / cingulum R	20 -50 6	7.688	<0.001
Calcarine R (BA17) / cingulum R	18 -60 18	6.541	0.002
Calcarine L (BA19) / cingulum L	-22 -54 8	7.801	<0.001
Calcarine L (BA17) / cingulum L	-16 -52 8	7.253	<0.001
Lingual R (BA18) / cingulum R	16 -48 4	7.951	<0.001
Lingual R (BA30) / cingulum R	14 -44 -4	7.049	0.001
Lingual L (BA19) / cingulum L	-16 -46 0	8.528	<0.001
Lingual L (BA27) / cingulum L	-12 -46 4	7.748	<0.001
Cuneus R (BA23)	18 -60 22	6.170	0.004
Cuneus L (BA17)	-18 -58 20	7.974	<0.001
Precuneus L (BA19) / cingulum L	-18 -50 4	8.360	<0.001
Fusiform R (BA19) / sagittal stratum R	30 -68 -16	8.790	<0.001
Fusiform R (BA37) / sagittal stratum R	38 -56 -18	8.562	<0.001
Fusiform L (BA37) / sagittal stratum L	-40 -52 -16	5.796	0.011
Fusiform L (BA19) / sagittal stratum L	-28 -68 -14	5.947	0.007
Temporal Inf R (BA20)	48 -38 -22	6.447	0.002
Temporal Inf L (BA20)	-44 -44 -16	5.290	0.048
Temporal Mid R (BA21)	56 -32 0	5.776	0.012
Rolandic Operc R (BA48) / sup longitudinal fasc R	42 -30 24	7.070	<0.001
Rolandic Operc L (BA48) / sup longitudinal fasc L	-36 -28 22	7.152	<0.001
Hippocampus R (BA20) / cingulum R	26 -20 -14	7.684	<0.001
Hippocampus R (BA35) / cingulum R	14 -8 -14	6.418	0.002
Hippocampus R (BA37)	34 -34 -2	6.520	0.002
Hippocampus L (BA20) / cingulum L	-26 -18 -16	5.448	0.030
Hippocampus L (BA37)	-34 -34 -2	5.372	0.039
Cingular cortex ant L (BA32) / cingulum L	-8 28 24	6.104	0.004
Cingular cortex ant R (BA32) / cingulum R	8 30 26	5.388	0.037
Frontal Mid L (BA46)	-26 38 28	6.214	0.003

Explanation of symbols: BA: Brodmann area; Coord.: coordinates, in millimetres, according to the Montreal Neurological Institute (MNI) standard reference space; *t*: test statistic as Student's *t*; *p* (corr): significance value, voxel-level (peak-level) corrected for the whole volume; ant, inf, mid, sup: anterior, inferior, middle, superior; operc: operculum, fasc: fasciculum; L, R: left, right. Conventions as in Table 1.

References

American Psychiatric Association, 1994. Diagnostic and statistic manual of mental disorders: DSM-IV. APA, Washington.

Antosik-Biernacka, A., Peuskens, H., De Hert, M., Peuskens, J., Sunaert, S., Van Hecke, P., Goraj, B., 2006. Magnetization transfer imaging in chronic schizophrenia. Med. Sci. Monit. 12, 17-21.

Ashburner, J., Friston, K., 1997. Multimodal image coregistration and partitioning--a unified framework. Neuroimage. 6, 209-217.

Ashburner, J., Friston, K.J., 2000. Voxel-based morphometry - the methods. Neuroimage. 11, 805-821.

Bachmann, S., Bottmer, C., Pantel, J., Schroder, J., Amann, M., Essig, M. , Schad, L.R., 2004. MRI-morphometric changes in first-episode schizophrenic patients at 14 months follow-up. Schizophr. Res. 67, 301-303.

Bachmann, S., Pantel, J., Flender, A., Bottmer, C., Essig, M., Schroeder, J., 2003. Corpus callosum in first-episode patients with schizophrenia - a magnetic resonance imaging study. Psychol. Med 33, 1019-27.

Bachmann, S., Bottmer, C., Schroder, J., Essig, M. , Magnotta, V., 2007. Compliance with medication but not structural MRI measures predict functional outcome in first-episode schizophrenia patients. Schizophr. Res. 90, 355-356.

Bagary, M.S., Symms, M.R., Barker, G.J., Mutsatsa, S.H., Joyce, E.M. , Ron, M.A., 2003. Gray and white matter brain abnormalities in first-episode schizophrenia inferred from magnetization transfer imaging. Arch. Gen. Psychiatry. 60, 779-788.

Bartzokis, G., Lu, P.H., Nuechterlein, K.H., Gitlin, M., Doi, C., Edwards, N., Lieu, C., Altshuler, L.L., Mintz, J., 2007. Differential effects of typical and atypical antipsychotics on brain myelination in schizophrenia. Schizophr. Res. 93, 13-22.

Beschoner, P., Riecker, A., Viviani, R., 2005. A review of magnetic resonance tomography findings in schizophrenia: Magnetization transfer ratio and diffusion-weighted imaging. Nervenheilkunde. 24, 190-197.

Bottmer, C., Bachmann, S., Pantel, J., Essig, M., Amann, M., Schad, L.R., Magnotta, V., Schroeder, J., 2005. Reduced cerebellar volume and neurological soft signs in first-episode schizophrenia. Psychiatry Res. 140, 239-50.

Cahn, W., Hulshoff Pol, H.E., Bongers, M., Schnack, H.G., Mandl, R.C., Van Haren, N.E., Durston, S., Koning, H., Van Der Linden, J.A., Kahn, R.S., 2002. Brain morphology in antipsychotic-naive schizophrenia: a study of multiple brain structures. Br. J. Psychiatry Suppl. 43, s66-72.

Di, X., Chan, R.C., Gong, Q.Y., 2009. White matter reduction in patients with schizophrenia as revealed by voxel-based morphometry: an activation likelihood estimation meta-analysis. Prog. Neuropsychopharmacol. Biol. Psychiatry. 33, 1390-1394.

Douaud, G., Smith, S., Jenkinson, M., Behrens, T., Johansen-Berg, H., Vickers, J., James, S., Voets, N., Watkins, K., Matthews, P.M. , James, A., 2007. Anatomically related grey and white matter abnormalities in adolescent-onset schizophrenia. Brain. 130, 2375-2386.

Filippi, M., Agosta, F., 2009. Magnetic resonance techniques to quantify tissue damage, tissue repair, and functional cortical reorganization in multiple sclerosis. Prog. Brain Res. 175, 456-482.

Foong, J., Symms, M.R., Barker, G.J., Maier, M., Woermann, F.G., Miller, D.H., Ron, M.A., 2001. Neuropathological abnormalities in schizophrenia: evidence from magnetization transfer imaging. Brain. 124, 882-892.

Friston, K. J., 1996. Statistical parametric mapping and other analyses of functional imaging data. In: A. W. Toga, A.W., Mazziotta, J.C. (Eds.), Brain Mapping: The Methods. Academic Press, New York.

Henkelman, R.M., Stanisz, G.J. , Graham, S.J., 2001. Magnetization transfer in MRI: a review. NMR Biomed. 14, 57-64.

Holmes, A.P., Blair, R.C., Watson, J.D. , Ford, I., 1996. Nonparametric analysis of statistic images from functional mapping experiments. J. Cereb. Blood. Flow Metab. 16, 7-22.

Honea, R.A., Crow, T.J., Passingham, D. , Mackay, C.E., 2005. Regional deficits in brain volume in schizophrenia: a meta-analysis of voxel-based morphometry studies. Am. J. Psychiatry. 162, 2233-2245.

Honea, R.A., Meyer-Lindenberg, A., Hobbs, K.B., Pezawas, L., Mattay, V.S., Egan, M.F., Verchinski, B., Passingham, R.E., Weinberger, D.R. , Callicott, J.H., 2008. Is gray matter volume an intermediate phenotype for schizophrenia? A voxel-based morphometry study of patients with schizophrenia and their healthy siblings. Biol. Psychiatry. 63, 465-474.

Konrad, A., Winterer, G., 2008. Disturbed structural connectivity in schizophrenia primary factor in pathology or epiphenomenon? Schizophr. Bull. 34, 72-92.

Kubicki, M., McCarley, R., Westin, C.F., Park, H.J., Maier, S., Kikinis, R., Jolesz, F.A., Shenton, M.E., 2007. A review of diffusion tensor imaging studies in schizophrenia. J. Psychiatr. Res. 41, 15-30.

Kubicki, M., Park, H., Westin, C.F., Nestor, P.G., Mulkern, R.V., Maier, S.E., Niznikiewicz, M., Connor, E.E., Levitt, J.J., Frumin, M., Kikinis, R., Jolesz, F.A., McCarley, R.W., Shenton, M.E., 2005. DTI and MTR abnormalities in schizophrenia: analysis of white matter integrity. Neuroimage. 26, 1109-1118.

Lieberman, J.A., Tollefson, G.D., Charles, C., Zipursky, R., Sharma, T., Kahn, R.S., Keefe, R.S., Green, A.I., Gur, R.E., McEvoy, J., Perkins, D., Hamer, R.M., Gu, H., Tohen, M., 2005. Antipsychotic drug effects on brain morphology in first-episode psychosis. Arch. Gen. Psychiatry. 62, 361-370.

Little, R.J.A., Rubin, D.B., 2002 Statistical Analysis with Missing Data, second ed. Wiley, New York.

Mandl, R.C., Schnack, H.G., Luigjes, J., van den Heuvel, M.P., Cahn, W., Kahn, R.S., Hulshoff Pol, H.E., 2010. Tract-based analysis of magnetization transfer ratio and diffusion tensor imaging of the frontal and frontotemporal connections in schizophrenia. Schizophr. Bull. 36, 778-787.

Mori, S., Wakana, S., Nagae-Poetscher, L.M. , van Zijl, P.C.M., 2005. MRI Atlas of Human White Matter. Elsevier, Amsterdam.

Nagai, M., Kishi, K., Kato, S., 2007. Insular cortex and neuropsychiatric disorders: a review of recent literature. Eur. Psychiatry. 22, 387-394.

Nichols, T.E., Holmes, A.P., 2002. Nonparametric permutation tests for functional neuroimaging: a primer with examples. Hum. Brain Mapp. 15, 1-25.

Oldfield, R. C., 1971. The assessment and analysis of handedness: The Edinburgh inventory. Neuropsychologia 9, 97-113.

Pomarol-Clotet, E., Canales-Rodriguez, E.J., Salvador, R., Sarro, S., Gomar, J.J., Vila, F., Ortiz-Gil, J., Iturria-Medina, Y., Capdevila, A. , McKenna, P.J., 2010. Medial prefrontal

cortex pathology in schizophrenia as revealed by convergent findings from multimodal imaging. Mol. Psychiatry. 15, 823-830.

Price, G., Cercignani, M., Chu, E.M., Barnes, T.R.E., Barker, G.J., Joyce, E.M., Ron, M.A., 2010. Brain pathology in first-episode psychosis: Magnetization transfer imaging provides additional information to MRI measurements of volume loss. NeuroImage 49, 185-192.

Scherk, H., Falkai, P., 2006. Effects of antipsychotics on brain structure. Curr Opin Psychiatry. 19, 145-150.

Shenton, M.E., Dickey, C.C., Frumin, M. , McCarley, R.W., 2001. A review of MRI findings in schizophrenia. Schizophr Res. 49, 1-52.

Van Essen, D.C., Dierker, D.L., 2007. Surface-based and probabilistic atlases of primate cerebral cortex. Neuron. 56, 209-225.

Viviani, R., Beschoner, P., Ehrhard, K., Schmitz, B. , Thone, J., 2007. Non-normality and transformations of random fields, with an application to voxel-based morphometry. Neuroimage. 35, 121-130.

Williams, L.M., 2008. Voxel-based morphometry in schizophrenia: implications for neurodevelopmental connectivity models, cognition and affect. Expert Rev. Neurother. 8, 1049-1065.

Wolff, S.D., Balaban, R.S., 1989. Magnetization transfer contrast (MTC) and tissue water proton relaxation in vivo. Magnetic Resonance in Medicine. 10, 135-144.

Worsley, K.J., Marrett, S. , Neelin, P. , Evans, A. C., 1992. A three-dimensional statistical analysis for CBF activation studies in human brain. J. Cerebr. Blood Flow Metab. 12, 900-918.

Wright, I.C., Rabe-Hesketh, S., Woodruff, P.W., David, A.S., Murray, R.M. , Bullmore, E.T., 2000. Meta-analysis of regional brain volumes in schizophrenia. American Journal of Psychiatry. 157, 16-25.

Zilles, K., Schleicher, A., Langemann, C., Amunts, K., Morosan, P., Palomero-Gallagher, N., Schormann, T., Mohlberg, H., Burgel, U., Steinmetz, H., Schlaug, G. , Roland, P.E., 1997. Quantitative analysis of sulci in the human cerebral cortex: Development, regional heterogeneity, gender difference, asymmetry, intersubject variability and cortical architecture. Human Brain Mapping. 5, 218-221.

Figures

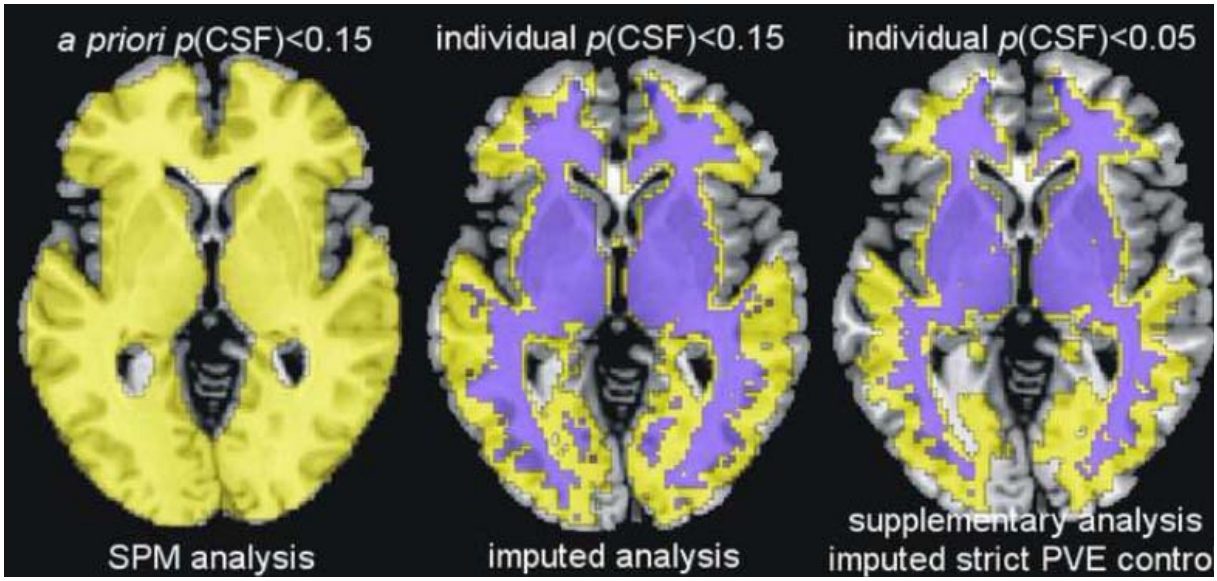

Figure 1

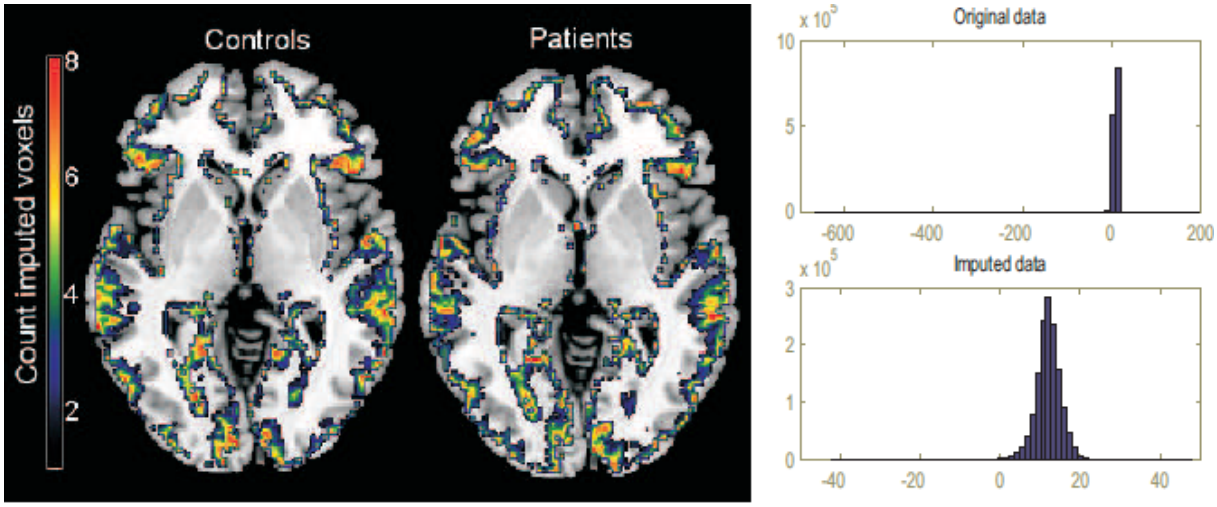
Controls
Patients
Count imputed voxels
8
6
4
2
x 10^5
Original data
10
5
0
-600
-400
-200
0
200
x 10^5
Imputed data
3
2
1
0
-40
-20
0
20
40

Figure 2

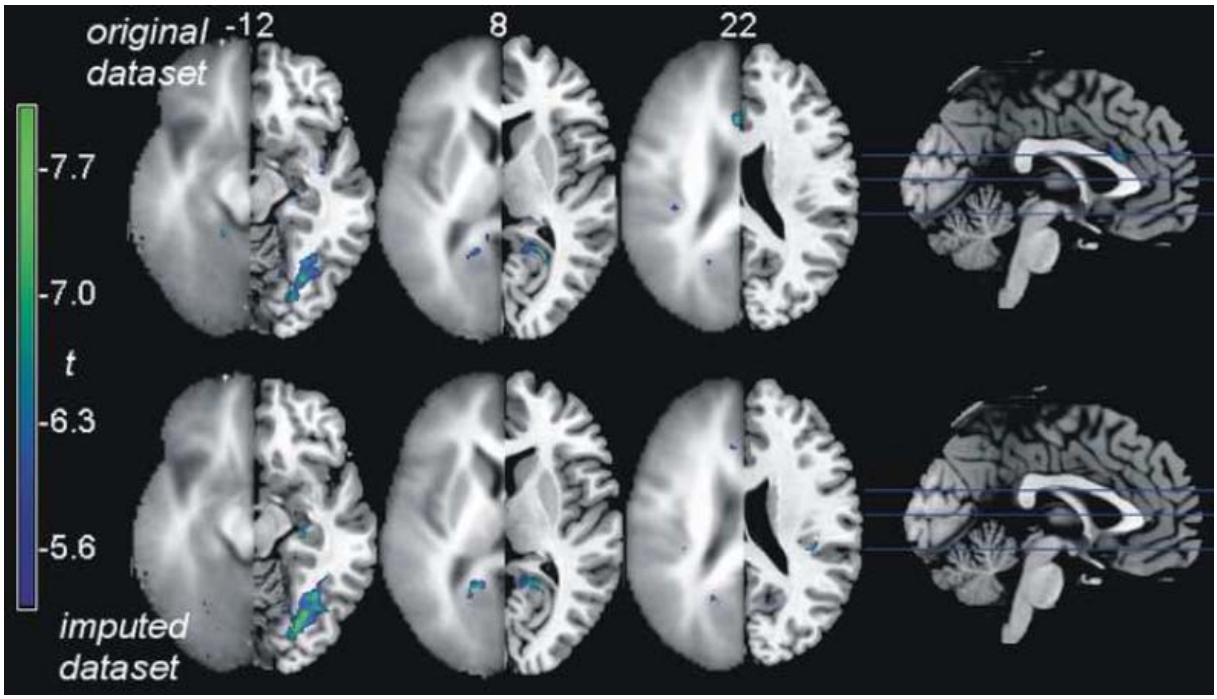

Figure 3